

Anomalous Coulomb-Enhanced Charge Transport in Triangular Triple Quantum Dots Systems

Shuo Dong ^a, Junqing Li ^a, Jianhua Wei ^{a*}

^a*School of Physics, The Renmin University of China, Beijing, 100876 China*

Abstract

Electron correlation and quantum interference are pivotal in mesoscopic transport. We theoretically study the nonequilibrium transport dynamics of a triangular triple quantum dot (TTQD) molecule connected to fermionic reservoirs using the exact hierarchical equations of motion (HEOM) formalism. We demonstrate a counter-intuitive transport signature where the stationary current is significantly enhanced by increasing the U , a behavior distinct from the suppression typically observed in linear quantum dot arrays. By analyzing the evolution of spectral functions, we attribute this enhancement to the interplay between Coulomb interaction-induced energy shifts and quantum interference effects unique to the triangular topology. We also explore how the circulation of chiral currents and electrode coupling strength modulates these interaction effects. Finally, we present a three-dimensional map of the transport current as a function of inter-dot tunneling (t) and Coulomb interaction (U), illustrating their combined effect on the current magnitude and its applications.

Keywords: berry phase, quantum dots, quantum computation

1. Introduction

Quantum dots (QDs), often described as “artificial atoms,” have become one of the most widely studied platforms in condensed matter physics and nanoscience. These nanoscale semiconductor structures confine electrons in all three spatial dimensions, yielding discrete, atom-like energy levels that are tunable through external gate voltages and magnetic fields [1, 2]. This tunability has made quantum dots a natural setting for studying fundamental quantum phenomena in controllable mesoscopic systems and for developing quantum technologies. The foundation of quantum dot physics was established through the experimental observation of single-electron charging effects. Meirav, Kastner, and Wind demonstrated periodic conductance resonances

in GaAs nanostructures, providing the first clear evidence of Coulomb blockade in quantum dots [3]. These pioneering experiments showed that when a quantum dot is weakly coupled to electron reservoirs, the addition energy required to place each successive electron on the dot produces a distinctive pattern of conductance peaks as a function of gate voltage. Kouwenhoven and colleagues further advanced the understanding of discrete energy levels and Coulomb charging effects, establishing quantum dots as true artificial atoms with shell structure [4, 5].

Central to quantum dot physics is the on-site Coulomb repulsion energy U , which characterizes the electrostatic cost of placing two electrons on the same dot. The theoretical framework for understanding U was established by Beenakker, who provided an early treatment of Coulomb blockade oscillations in quantum dot conductance [6]. In the Hubbard model description of quantum dots [7], U

Email address: corresponding author: wjh@ruc.edu.cn
(Jianhua Wei ^{a*})

competes directly with the kinetic energy scale set by the interdot tunneling amplitude t . When $U \ll t$, electrons delocalize freely and transport is relatively unimpeded. As U increases toward and beyond t , charge fluctuations become energetically costly, electrons tend to localize on individual dots, and the system enters a strongly correlated regime in which conventional single-particle descriptions break down. This competition between U and t is a genuine control parameter that drives the system through qualitatively different physical regimes, from weakly interacting Fermi liquid behavior to strongly correlated Mott-like insulating states. How U shapes transport properties is thus a central issue in quantum dot physics. Loss and DiVincenzo’s seminal proposal established electron spins confined in quantum dots as viable qubits, highlighting their long coherence times and gate-voltage controllability as key advantages for scalable quantum computation [8]. Following this proposal, subsequent experiments demonstrated precise control over individual and coupled spin qubits [9, 10, 11, 12]. These developments established quantum dots as leading candidates for solid-state quantum computing, and simultaneously underscored the importance of understanding Coulomb interactions, since U directly governs the exchange splitting between singlet and triplet spin states that underpins spin qubit operation.

Linear quantum dot arrays, from double quantum dots (DQDs) to triple quantum dots (TQDs) systems, have been extensively studied as building blocks for quantum computation and as platforms for exploring interdot coupling, tunneling dynamics, and multi-qubit operations. For DQDs, Van der Wiel et al. provided a comprehensive review of electron transport, discussing the interplay among interdot tunneling, lead coupling, and Coulomb interactions [13]; coherent charge oscillations were demonstrated by Hayashi et al. [14], and the Pauli spin blockade was observed by Ono et al. and Johnson et al. [15, 16]. Extending to TQDs, Schröer et al. realized electrostatically defined serial devices with controllable electron numbers [19], while Gaudreau

and colleagues fabricated tunable few-electron TQDs and observed coherent three-dot coupling [20, 21]; the transport theory was further developed by Rogge and Haug, who highlighted quantum interference between different tunneling pathways [22, 23], and by Michaelis et al. using rate equations [24]. Across both DQD and linear TQD configurations, the role of the on-site Coulomb interaction U is qualitatively consistent: stronger repulsion raises the addition energy, widens the Coulomb blockade valleys, localizes electrons on individual dots, and suppresses sequential tunneling, reinforcing the conventional expectation that U impedes rather than facilitates current flow.

Moving beyond linear quantum dots, triangular triple quantum dots (TTQDs) systems are particularly intriguing because they break linear symmetry and introduce geometric frustration, potentially giving rise to novel quantum phenomena. The threefold rotational symmetry of triangQDs creates fundamentally different interference conditions compared to linear arrangements. Korkusinski et al. investigated the electronic properties of triangular lateral quantum dot molecules and introduced “topological Hund’s rules” to describe state filling [25], showing that geometry alone can qualitatively alter the energy spectrum and charge configurations. Experimentally, Granger et al. mapped out the three-dimensional transport diagram of a TQD, revealing complex charge stability regions in multi parameter space [26]. Seo et al. demonstrated charge frustration effects in a triangular TQD arising from the geometric arrangement [27], showing that the triangular geometry leads to degenerate charge configurations and non-trivial ground states that differ qualitatively from linear arrangements. On the theoretical side, Žitko, Bonča, and Pruschke investigated quantum phase transitions in TQDs using numerical renormalization group methods, finding that the interplay between Kondo screening and geometric structure can lead to complex phase diagrams [28].

Yet despite this extensive body of work, a basic question about transport in triangular TQDs has not been exam-

ined systematically. For single dots and linear multi-dot systems, it is well established that increasing by making charge fluctuations energetically costly and driving the system toward electron localization[29, 30, 31]. However, this picture was developed primarily for systems with simple, effectively one-dimensional tunneling topologies, in which a single dominant transport pathway exists and U acts uniformly to block it. The triangular TQD geometry violates this assumption in a fundamental way. With three dots arranged in a closed loop, electrons have access to multiple interfering paths whose phase relationships are not fixed by geometry alone but are renormalized by interactions. The closed-loop structure introduces a topological character analogous to Aharonov-Bohm physics even in the absence of external magnetic fields. Geometric frustration prevents the simultaneous optimization of all pairwise interactions, potentially stabilizing unusual ground states. The absence of left-right mirror symmetry distinguishes the triangular configuration from all linear arrangements and removes constraints that would otherwise pin the interference conditions. These features together raise a question that has not been addressed: does increasing U suppress conductance in a triangular TQD as in simries, or can the interplay between strong Coulomb correlations and closed-loop topology produce qualitatively different behavior?

Addressing this question matters both for fundamental reasons and for practical ones. Identifying a regime in which strong correlations enhance rather than suppress transport would pointopic physics, one that expands our understanding of how electron-electron interactions operate in confined geometries. At the same time, quantum dot arrays are actively being developed for quantum simulation, computation, and sensing, and triangular geometries are increasingly explored as building blocks for two-dimensional quantum dot arrays. If U can enhance conductance in such geometries, this opens a design principle for interaction-controlled quantum devices. For TQD-based qubits specifically, understanding how U affects transport and coherence

across a wide parameter range is essential for device optimization, since qubit operation requires precise control over both charge and spin degrees of freedom that U directly governs.

In this work, we investigate the transport properties of a triangular TQD across a wide range of Coulomb interaction strengths using hierarchical equations of motion (HEOM) method. Our central finding is that increasing the on-site Coulomb repulsion U enhances conductance through the system, in stark contrast to the conventional expectation that stronger interactions suppress current flow. This effect is intrinsically tied to the closed-loop triangular geometry and does not arise in linear TQD configurations, confirming that the interplay between U and geometric structure drives the phenomenon. Our results demonstrate a mechanism by which strong correlations can be harnessed constructively, with potential implications for interaction-controlled quantum devices and for the broader understanding of correlated transport in geometrically frustrated systems.

2. Theory and Methoed

The theoretical treatment of transport through interacting quantum dot systems in the nonequilibrium regime requires sophisticated many-body techniques.

The system consists of three quantum dots arranged in a triangular geometry, as shown in figure 1(a), where all on-site energies and intra-dot Coulomb interactions are identical, and the inter-dot hopping amplitude t is uniform across all three links. Two of the three quantum dots (labeled dot 1 and dot 3) are each coupled to a separate fermionic electron reservoir, and a small bias voltage V is applied between the two reservoirs to drive a transport current through the system. Another quantum dot (dot 2) is not directly coupled to any reservoir but participates in transport indirectly through its hybridization with dots 1 and 3. Throughout the calculation, electron-hole symmetry is maintained by setting the on-site energy $\varepsilon_d = -U/2$, where U is the Coulomb interaction strength.

The Anderson impurity model provides the theoretical framework for studying this system, in the multi-impurity generalization, each quantum dot is characterized by an on-site energy level, an intra-dot Coulomb repulsion U , and hybridization both with neighboring dots through hopping t and with the continuum of conduction electrons in the attached reservoirs. The Hamiltonian of the full system can be written as

$$H = H_{\text{dots}} + H_{\text{leads}} + H_{\text{hyb}}, \quad (1)$$

where H_{dots} contains the on-site energies, the Coulomb repulsion, and the inter-dot hopping among all three dots:

$$H_{\text{dots}} = \sum_{i\mu} \varepsilon_i \hat{d}_{i\mu}^\dagger \hat{d}_{i\mu} + U \sum_i \hat{n}_{i\uparrow} \hat{n}_{i\downarrow} + \sum_{i \neq j \mu} t_{ij} \hat{d}_{i\mu}^\dagger \hat{d}_{j\mu}. \quad (2)$$

The $\hat{d}_{i\mu}^\dagger$ ($\hat{d}_{i\mu}$) in above fomula is creation(annihilation) operator for an electron with μ spin on the i -th dot. H_{leads} describes the two noninteracting electron reservoirs:

$$H_{\text{leads}} = \sum_{\alpha k \mu} \varepsilon_{\alpha k} c_{\alpha k \mu}^\dagger c_{\alpha k \mu}, \quad (3)$$

$c_{\alpha k \mu}^\dagger$ ($c_{\alpha k \mu}$) is creation(annihilation) operator for electron of lead α on the k -th state, and $\varepsilon_{\alpha k}$ is the energy of an electron with wave vector k in the α lead. And H_{hyb} captures the tunnel coupling between dots 1 and 3 and their respective leads:

$$H_{\text{hyb}} = \sum_{\alpha k i \mu} V_{\alpha k i \mu} \hat{d}_{i\mu}^\dagger c_{\alpha k \mu} + H.c., \quad (4)$$

with $V_{\alpha k i \mu}$ being the tunnel matrix element between i -th impurity and electrons with k -th state on the α -reservoir. For this paper, $V_{\alpha k \mu}$ is the electron tunneling strength between two leads. The effect of electron reservoirs on QDs is taken into account through the hybridization functions, $\Delta_{\mu\nu}(\omega) \equiv \Sigma_\alpha \Delta_{\alpha\mu\nu}(\omega) = \pi \Sigma_{\alpha k} V_{\alpha\mu k} V_{\alpha\nu k}^* \delta(\omega - \varepsilon_{\alpha k})$, in the absence of applied chemical potentials. Generally, we adopt Lorentzian hybridization functions in the HEOM approach, that is, $\Delta_{\mu\nu}(\omega) = \delta_{\mu\nu} \Delta W^2 / (\omega^2 + W^2)$, with $\Delta = \Sigma_\alpha \Delta_\alpha$ being the overall dot-lead coupling strength and W is the bandwidth of the electrodes.

A magnetic flux ϕ threading the lead-free triangular loop modifies the inter-dot hopping amplitude through a phase factor. We use perturbation theory in the inter-dot tunneling t , treating it as small compared to the on-site Coulomb repulsion U . This approach allows us to derive an effective spin-exchange Hamiltonian from the microscopic quantum dot Hamiltonian H_{dots} [32, 33] by integrating out high-energy charge excitations. The resulting Hamiltonian takes the form:

$$H_{\text{eff}} = -t(1-n) \sum_{j k, \mu} \left(\hat{d}_{j\mu}^\dagger \hat{d}_{k\mu} + \text{H.c.} \right) + J \sum_{j < k} \left(\hat{\mathbf{S}}_j \hat{\mathbf{S}}_k - \frac{1}{4} \hat{n}_j \hat{n}_k \right) + \chi \hat{\mathbf{S}}_1 \left(\hat{\mathbf{S}}_2 \times \hat{\mathbf{S}}_3 \right), \quad (5)$$

where n is the the expectation value of the occupation number per dot, and $\hat{n}_j = \hat{d}_j^\dagger \hat{d}_j$ is the number operator for electrons on dot j . $\hat{\mathbf{S}}_1$, $\hat{\mathbf{S}}_2$ and $\hat{\mathbf{S}}_3$ are the spin operators on quantum dots, and $\mathbf{S}_j = \frac{1}{2} \sum_{\mu, \mu'} \hat{d}_{j\mu}^\dagger \boldsymbol{\tau}_{\mu\mu'} \hat{d}_{j\mu'}$, $\boldsymbol{\tau}_{\mu\mu'}$ are the Pauli matrices. The first term will vanish in the half-filling situation ($n = 1$). The second term is Heisenberg exchange interaction with $J = 4t^2/U$. The third term is the chiral term with chiral operator[41] $\hat{\mathbf{S}}_1 \cdot \left(\hat{\mathbf{S}}_2 \times \hat{\mathbf{S}}_3 \right)$, where χ is the chiral interaction with $\chi = 24t^3 \sin(2\pi\phi/\phi_0)/U^2$, and ϕ is the magnetic flux enclosed by the TTQD structure. Here, $\phi_0 = hc/e$ is the unit of quantum flux. For simplicity, we let $\varphi = 2\pi\phi/\phi_0$; thus, $\chi = 24t^3 \sin(\varphi)/U^2$.

The hierarchical equations of motion(HEOM) approach examines quantum dot properties in equilibrium and nonequilibrium states through the reduced density operator, which possesses a universal formalism applicable to arbitrary system Hamiltonians. It can accurately solves the three-impurity Anderson model[34]. Recent progress has substantially broadened HEOM's scope and efficiency for quantum transport applications. Tanimura offered a comprehensive review of theoretical foundations and numerical implementations for both bosonic and fermionic systems, emphasizing its advantages over perturbative master equation approaches in strong-coupling regimes[37].

These developments establish HEOM as a reliable tool for exploring thermoelectric phenomena in multi-dot systems.

The HEOM framework derives from Feynman-Vernon influence functional path-integral theory[35] and employs Grassmann algebra for fermionic dissipation[36]. Consequently, HEOM provides formally exact treatment of general open systems coupled to reservoir baths satisfying Grassmann Gaussian statistics. The mathematical construction has been comprehensively discussed in previous references.[38, 39, 40] Here, we highlight key features particularly relevant to the quantum dot systems examined in this work's main text.

The HEOM approach provides a universal framework for investigating quantum dot properties under equilibrium and non-equilibrium conditions through the reduced density operator, applicable to arbitrary system Hamiltonians. We present a concise derivation below. At time t , the reduced density operator of the system is defined as $\rho(t) = \text{tr}_{\text{res}} \rho_{\text{T}}(t)$, where $\rho_{\text{T}}(t)$ denotes the total density operator of both system and reservoirs. The reduced density operator $\rho(t)$ connects to its initial value at time t_0 through the reduced Liouville-space propagator $\mathcal{G}(t, t_0)$:

$$\rho(t) = \mathcal{G}(t, t_0) \rho(t_0). \quad (6)$$

Using the Feynman-Vernon influence functional formalism, the path-integral representation of the reduced Liouville-space propagator takes the form

$$\mathcal{G}(\psi, t; \psi_0, t_0) = \int_{\psi_0[t_0]}^{\psi[t]} \mathcal{D}\psi e^{iS[\psi]} \mathcal{F}[\psi] e^{-iS[\psi']}, \quad (7)$$

where $S[\psi]$ denotes the classical action of the reduced system and $\mathcal{F}[\psi]$ is the corresponding influence functional. Following the work of Zhenhua Li et al.[42], we invoke Wick's theorem together with Grassmann algebra to express the influence functional $\mathcal{F}[\psi]$ as

$$\mathcal{F}[\psi] = \exp \left\{ - \int_0^t d\tau \mathcal{R}[\tau, \{\psi\}] \right\}, \quad (8)$$

where $\mathcal{R}[\tau, \{\psi\}] = \frac{i}{\hbar^2} \sum_{\alpha i \mu \sigma} \mathcal{A}_{ij\mu}^{\bar{\sigma}}[\psi(t)] \mathcal{B}_{\alpha i \mu}^{\sigma}[t, \psi]$, with $\sigma = +, -$ and $\bar{\sigma} = -\sigma$. The Grassmann variables $\mathcal{A}_{i\bar{s}}^{\bar{\sigma}}$ and $\mathcal{B}_{\alpha i \mu}^{\sigma}$ are defined as

$$\mathcal{A}_{i\bar{s}}^{\bar{\sigma}}[\psi(t)] = d_{i\bar{s}}^{\bar{\sigma}}[\psi(t)] + d_{i\bar{s}}^{\sigma}[\psi'(t)], \quad (9)$$

$$\mathcal{B}_{\alpha i \mu}^{\sigma}[t, \psi] = -i [B_{\alpha i \mu}^{\sigma}(t, \psi) - B_{\alpha i \mu}^{\prime\sigma}(t, \psi')], \quad (10)$$

with

$$\begin{aligned} B_{\alpha i \mu}^{\sigma}(t, \psi) &= \sum_j \int_0^t d\tau C_{\alpha i j \mu}^{\sigma}(t - \tau) d_{j\mu}^{\sigma}[\psi(\tau)], \\ B_{\alpha i \mu}^{\prime\sigma}(t, \psi') &= \sum_j \int_0^t d\tau C_{\alpha i j \mu}^{\sigma*}(t - \tau) d_{j\mu}^{\sigma}[\psi'(\tau)]. \end{aligned} \quad (11)$$

Here, $C_{\alpha i j \mu}^{\sigma}(t)$ represents the reservoir correlation functions. In the present computational scheme, $C_{\alpha i j \mu}^{\sigma}(t)$ is decomposed into a sum of exponential terms by combining the fluctuation-dissipation theorem with the Cauchy residue theorem and the Padé spectral decomposition[43] of the Fermi function:

$$C_{\alpha i j \mu}^{\sigma}(t) = \sum_{m=1}^M \eta_{\alpha i j \mu m}^{\sigma} e^{-\gamma_{\alpha i j \mu m}^{\sigma} t}. \quad (12)$$

The bath effects enter the equations of motion through M exponential terms. The auxiliary density operators (ADOs) $\{\rho_j^n = \rho_{j_1 \dots j_n}\}$ are determined by the time derivative of the influence functional. The composite index $j \equiv (\sigma \mu m)$ characterizes the transfer of an electron to or from ($\sigma = +/ -$) the impurity state μ , while $n = 1, 2, \dots, L$ specifies the truncation tier level. In the present study, setting $L = 4$ is found sufficient for obtaining numerically exact results. The resulting hierarchy equations of motion can be written in the following compact form:

$$\begin{aligned} \dot{\rho}_{j_1 \dots j_n}^{(n)} &= - \left(i\mathcal{L} + \sum_{r=1}^n \gamma_j \right) \rho_{j_1 \dots j_n}^{(n)} - i \sum_j \mathcal{A}_j \rho_{j_1 \dots j_n}^{(n+1)} \\ &\quad - i \sum_{r=1}^n (-)^{n-r} \mathcal{C}_{j_r} \rho_{j_1 \dots j_{r-1} j_{r+1} \dots j_n}^{(n-1)}. \end{aligned} \quad (13)$$

In the above, \mathcal{L} is the Liouvillian superoperator of the quantum dots, which incorporates electron-electron inter-

actions, and is defined as $\mathcal{L} \equiv [H_{\text{dot}}, \cdot]$. The Grassmanian superoperators $\mathcal{A}_{\bar{j}} \equiv \mathcal{A}_{i_s}^{\bar{\sigma}}$ and $\mathcal{C}_j \equiv \mathcal{C}_{ij_{sm}}^{\sigma}$ act on an arbitrary operator \hat{O} according to $\mathcal{A}_{\bar{j}}\hat{O} \equiv [\hat{d}_{i_s}^{\bar{\sigma}}, \hat{O}]$ and $\mathcal{C}_j\hat{O} \equiv \eta_j \hat{d}_{i_s}^{\sigma} \hat{O} + \eta_j^* \hat{O} \hat{d}_{i_s}^{\sigma}$, respectively.

Furthermore, only the first-tier auxiliary density operators are required to accurately evaluate the transient current flowing through electrode α :

$$I_{\alpha}(t) = i \sum_{i\mu} \text{tr}_{\text{sys}} \left[\rho_{\alpha i\mu}^{\dagger}(t) \hat{d}_{i\mu} - \hat{d}_{i\mu}^{\dagger} \rho_{\alpha i\mu}^{-}(t) \right]. \quad (14)$$

In addition, the spectral function is obtained by propagating the correlation functions $C_{a_{i\mu} a_{i\mu}^{\dagger}}(t)$ and $C_{a_{i\mu}^{\dagger} a_{i\mu}}(t)$ in time and subsequently performing a semi-infinite Fourier transform. This procedure directly yields the spectral function $A_{i\mu}(\omega)$ associated with spin μ in the i -th quantum dot. The fluctuation-dissipation theorem further allows the spectral density function of the quantum dots to be extracted from these correlation functions. The spectral function is given by

$$A_{i\mu}(\omega) = \frac{1}{\pi} \text{Re} \left\{ \int_0^{\infty} dt \left\{ C_{a_{i\mu} a_{i\mu}^{\dagger}}(t) + \left[C_{a_{i\mu}^{\dagger} a_{i\mu}}(t) \right]^* \right\} e^{-i\omega t} \right\}. \quad (15)$$

3. Results and Discussion

Figure 1 presents a comparison of the transport current as a function of U for the triangular triple quantum dots (TTQDs) and linear triple quantum dots (LTQDs) configurations, with all other parameters held identical and the inter-dot hopping fixed at $t = 0.25$ meV. In the linear triple quantum dot arrangement, where only nearest-neighbor hopping is present and the three dots form a chain, the transport current decreases monotonically as U increases from $2t$ to $5t$. This monotonic suppression is consistent with the standard expectation from the Anderson impurity model in the strong-coupling regime. In striking contrast, the triangular triple quantum dot system exhibits a pronounced non-monotonic dependence of the transport current on U . Starting from $U = 2t$, the current first increases

with U , reaches a maximum at approximately $U = 3.5t$, and subsequently decreases for larger values of U . This non-monotonic behavior represents the central finding of this work and signals the presence of a mechanism that, over a certain range of Coulomb interaction, enhances the transport current despite the growing on-site repulsion.

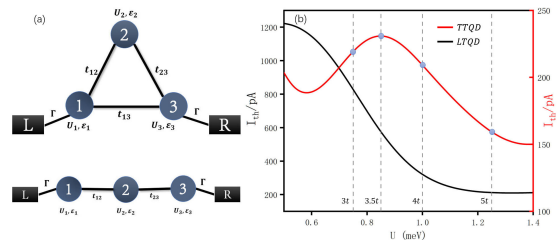


Figure 1: (a) Schematic diagrams of a triangular triple quantum dots (TTQDs) and a linear triple quantum dots (LTQDs), Quantum dot 1 and quantum dot 3 are connected to the left and right electrodes. (b) Comparison of the transport current as a function of the on-site Coulomb interaction U for the TTQDs and LTQDs configurations. The filled markers on the TTQD curve denote the specific values of U at which the spectral function $A(\omega)$ has been explicitly evaluated, with all other parameters held identical and the inter-dot hopping fixed at $t = 0.25$ meV. The other parameters are set as follows: $k_B T = 0.1$ meV, $\Gamma = 0.025$ meV, $V = 0.1$ meV

To elucidate the mechanism underlying the non-monotonic current, we compute the frequency-resolved spectral function $A(\omega)$ at several representative values of U along both the ascending and descending portions of the current curve, as shown in figure 2. Within the small-bias regime, the current is predominantly controlled by the spectral weight available inside the conducting window around the Fermi level, which is shown by the dotted line in Figure 2. For clarity, we restrict our presentation to the spectral weight in the vicinity of the Fermi level $\omega = 0$.

At the smallest value of U considered, both spectral peaks reside below the Fermi level. As U increases beyond $2t$, a systematic evolution of the spectral function is observed. The right peak, being the one closest to the Fermi level, begins to shift toward the Fermi energy. Simultaneously, the spectral weight of the right peak decreases while that of the left peak increases. This redistribution

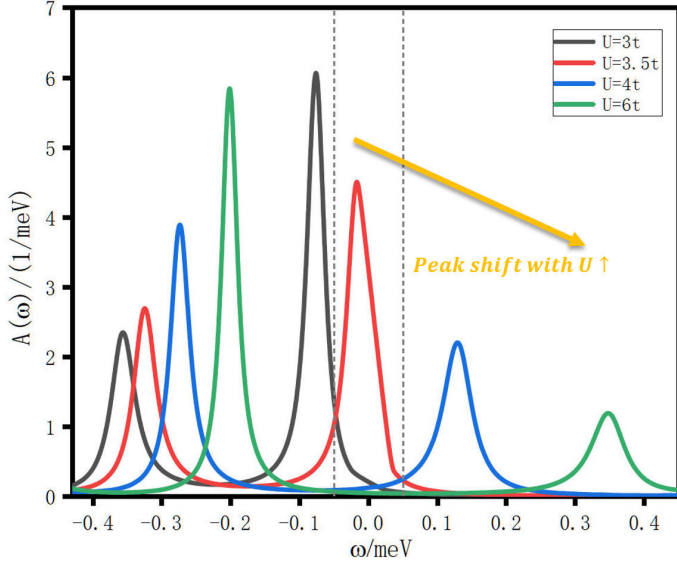


Figure 2: Spectral function $A(\omega)$ of the triangular triple quantum dot system in the vicinity of the Fermi level $\omega = 0$, computed at representative on-site Coulomb interaction U selected from both the rising and the falling portions of the current curve in Fig. 1.

of spectral weight between the two peaks is a hallmark of correlation-driven restructuring of the electronic spectrum. In the presence of Coulomb interactions, the eigenstates of the system are no longer simple single-particle states but rather correlated many-body states that incorporate the effects of electron-electron repulsion. The energy of these states depends on both the kinetic energy associated with interdot hopping and the potential energy arising from Coulomb repulsion. As U increases, states with lower total Coulomb energy become relatively more favorable, and the system reorganizes its spectral weight to reflect this energetic preference. In the triangular geometry, certain many-body states correspond to charge configurations where electrons are distributed to minimize mutual repulsion while maintaining connectivity to the leads. These states can have energies that increase less rapidly with U than other states, or in some cases, their energies relative to the Fermi level may even decrease due to the specific form of the interaction Hamiltonian in the triangular topology. This differential energy shift causes spectral peaks to move toward the Fermi level, enhancing transport when they

enter the conducting window.

The non-monotonic behavior of the current is directly explained by the trajectory of the right spectral peak relative to the bias window centered at the Fermi level. At $U = 3t$, the right peak has shifted to a position near $\omega = -0.08t$, while the left peak resides at $\omega = -0.35t$. The right peak is now in close proximity to the Fermi level, and its spectral weight, although reduced compared to its value at $U = 2t$, still contributes significantly to the transport. As U continues to increase and reaches $U = 3.5t$, the right peak arrives in the immediate vicinity of the Fermi level. At this point the left peak resides at $\omega = -0.31t$, having also shifted toward the Fermi level compared to its earlier position, but remaining well outside the narrow conducting window defined by the small applied bias. The transport current attains its maximum value at $U = 3.5t$ precisely because the antibonding spectral resonance is optimally aligned with the bias window. Physically, the antibonding spectral resonance, driven toward the Fermi level by the increasing Coulomb repulsion, sweeps through the narrow conducting window. The alignment of this resonance with the Fermi level maximizes the transmission probability and, consequently, the current. For U larger than $3.5t$, the right peak continues to shift and eventually crosses the Fermi level, moving out of the conducting window on the opposite side. At the same time, the ongoing suppression of the spectral weight of this peak by the growing Coulomb repulsion further reduces its contribution to the current. The combined effect of the peak moving away from the optimal position and losing spectral weight produces the observed decrease in the transport current at large U . Although the left peak continues to approach the Fermi level slowly, but never enters the bias window, and its growing spectral weight cannot compensate for the loss of the right peak contribution. The physical mechanism driving this energy shift involves the interplay between Coulomb repulsion and the quantum interference inherent to the triangular geometry. In the triangular configuration, electrons can traverse

between the two connected dots either directly through the interdot hopping or indirectly via the unconnected third dot. These two pathways interfere, and the relative phase between them depends on the energy spectrum of the system. Coulomb interactions modify the energy levels of the many-body states, thereby altering the interference conditions. In systems with quantum interference, the position of transmission resonances depends sensitively on the phase relationships between different transport pathways. Coulomb interactions introduce energy-dependent phase shifts that can tune these resonances into alignment with the Fermi level. This tuning effect is absent in linear geometries, where the lack of alternative pathways prevents the formation of interference-based resonances that can be manipulated by interactions.

To assess the robustness of this interpretation, we present in Figure 3 the transport current as a function of U for several values of the dot-electrode coupling strength Γ .

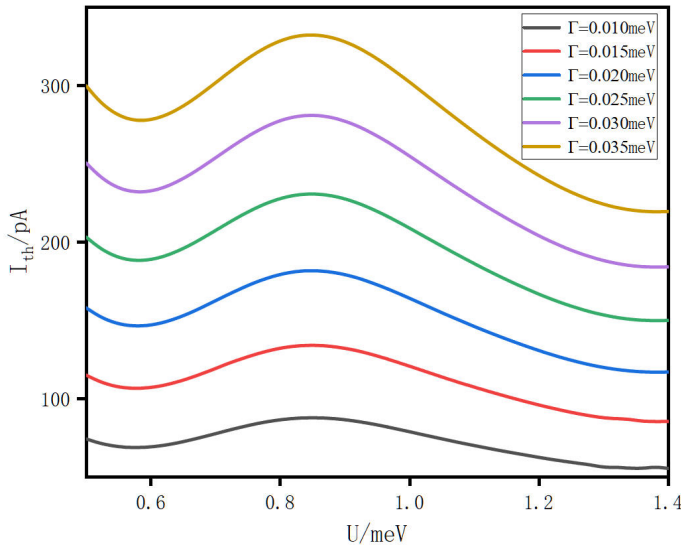


Figure 3: (Transport current I through the triangular triple quantum dot as a function of the on-site Coulomb interaction U , computed for several values of the lead-dot hybridization strength Γ .

Increasing Γ systematically raises the magnitude of the transport current across the entire range of U , which is physically expected, a larger Γ broadens the quasiparticle resonances and increases the tunneling rate, thereby

enhancing the current for any given alignment between the spectral peak and the transport window. The qualitative non-monotonic structure of the I - U curve is, however, preserved for all values of Γ examined. The position of the current maximum shifts only weakly with Γ , consistent with the fact that the peak migration in energy is controlled by the many-body self-energy and is therefore primarily a function of U/t rather than of Γ .

Reducing Γ diminishes the current amplitude and sharpens the spectral features, but again leaves the essential U -dependence unchanged. This insensitivity of the current's qualitative behavior to Γ is an important consistency check: it confirms that the non-monotonic current is not an artifact of a particular coupling regime but is a robust property of the triangular topology and the associated chiral level renormalization. The spectral function analysis of Fig. 2 and the coupling-strength sweep of Fig. 3 together provide a consistent account of the anomalous current enhancement. The triangular geometry generates chiral quasiparticle states whose energies are pulled toward the Fermi level by the Coulomb interaction; as these states pass through the transport window, the current rises and then falls. This behavior persists across a wide range of Γ , confirming that it reflects the topology of the system rather than any fine-tuning of parameters.

To characterize the robustness of the anomalous current enhancement, we compute the transport current I_{th} as a function of both U and t over a wide range of parameters. The results are summarized in Figure 4, which presents a three-dimensional plot of the threshold current I_{th} in the t - U plane. The three-dimensional surface shows nontrivial structure. The yellow arrow in the figure traces a path of fixed t along which U increases, corresponding to the direction of current enhancement described in the previous section. Following the yellow arrow, the current rises from its value at small U , reaches a maximum, and then falls along the trajectory indicated by the blue arrow. The non-monotonic U -dependence of the current at fixed t is

thus consistently observed across the full range of t values explored, confirming that the phenomenon is not limited to a specific choice of hopping amplitude but is a generic feature of the TTQD geometry.

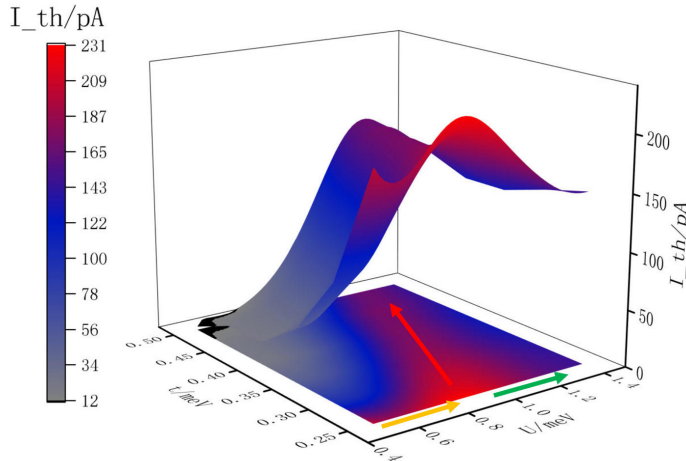


Figure 4: Three-dimensional representation of transport current as a function of interdot hopping amplitude t and on-site Coulomb repulsion U for the triangular triple quantum dot system. Yellow arrows indicate regions where transport current increases with growing U , demonstrating the counterintuitive enhancement effect. Blue arrows mark regions where further increases in U suppress the current due to Coulomb blockade effects. Red arrows highlight the trend that larger values of t require correspondingly larger values of U to achieve maximum transport current, revealing that the phenomenon is governed by the dimensionless ratio U over t . The plot demonstrates that interaction-enhanced transport occurs in an intermediate regime where U and t are comparable in magnitude.

The red arrow in Figure 4 reveals a systematic trend of particular physical significance, as t increases, the value of U at which the current reaches its maximum also increases. This means that the current peak shifts to larger U as the hopping amplitude grows. The implication is that the anomalous current enhancement is a phenomenon governed by the interplay between t and U through their ratio, rather than by either parameter independently. This phenomenon has an important physical corollary. It means that the current enhancement is not a perturbative effect that vanishes at small U/t , nor is it a strong-coupling phenomenon that only appears at $U \gg t$. Instead, it occurs in an intermediate coupling regime where both kinetic and interaction energy

scales are comparable, and where quantum interference in the triangular loop and Coulomb-driven renormalization of the chiral state energies cooperate to produce the anomalous transport signature. The linear geometry, lacking the loop structure, cannot support the closed-loop virtual processes that drive the orbital renormalization, and therefore shows no such enhancement regardless of the U and t .

4. Summary and Conclusions

In this work, we have studied transport through a triangular triple quantum dot system. The central finding of this study is the counterintuitive non-monotonic dependence of the transport current on the on-site Coulomb interaction U . While a linear triple quantum dot under otherwise identical conditions shows a monotonically decreasing current as U increases, the triangular system exhibits a clear current enhancement as U is increased from moderate values, followed by a decrease at larger U . Spectral function analysis reveals that Coulomb repulsion drives certain many-body states toward the Fermi level, increasing their contribution to transport when they enter the conducting window defined by the bias voltage. Finally, by mapping the transport current across a wide range of both U and t , we have demonstrated that the current enhancement is governed not by either parameter alone but by the combined effect of U and t . These results suggest that the triangular quantum dot geometry may serve as a useful experimental platform for engineering interaction-tunable transport responses, in which the current through the device can be increased rather than suppressed by strengthening the on-site Coulomb repulsion, provided the hopping amplitude and interaction strength are tuned to the appropriate intermediate-coupling regime.

The principle identified in this work, is not limited to the specific triangular three-dot geometry. More complex loop-containing networks, including tetrahedral four-dot clusters, ladder geometries, and two-dimensional arrays with embedded loops, are all expected to exhibit analogous

interaction-driven spectral renormalization effects arising from the closed-loop virtual hopping processes identified here. As the network size and connectivity increase, the number of independent chiral channels grows, and the interplay between frustration, interaction, and interference is expected to give rise to increasingly rich transport phenomenology. The present work provides both the conceptual framework and the specific spectral mechanism needed to analyze and interpret these more complex cases, and it motivates a systematic study of how the topology of the dot network determines the sign and magnitude of the interaction-driven current correction across a broader class of correlated nanoscale conductors.

5. Acknowledgements

The support from the Natural Science Foundation of China (Grant Nos. 12274454, 11774418, 11374363, 11674317, 11974348, 11834014 and 21373191), the Strategic Priority Research Program of CAS (Grants No. XDB28000000 and No. XDB33000000), the Training Program of Major Research plan of NSFC (Grant No. 92165105).

6. Data Availability

The data that support the findings of this study are available from the corresponding author upon reasonable request.

References

- [1] L. P. Kouwenhoven, C. M. Marcus, P. L. McEuen, S. Tarucha, R. M. Westervelt, and N. S. Wingreen, "Electron transport in quantum dots," in *Mesoscopic Electron Transport*, edited by L. L. Sohn, L. P. Kouwenhoven, and G. Schön (Kluwer, Dordrecht, 1997), pp. 105-214.
- [2] R. C. Ashoori, "Electrons in artificial atoms," *Nature* 379, 413 (1996).
- [3] U. Meirav, M. A. Kastner, and S. J. Wind, "Single-electron charging and periodic conductance resonances in GaAs nanostructures," *Phys. Rev. Lett.* 65, 771 (1990).
- [4] L. P. Kouwenhoven, T. H. Oosterkamp, M. W. S. Danoesastro, M. Eto, D. G. Austing, T. Honda, and S. Tarucha, "Excitation spectra of circular, few-electron quantum dots," *Science* 278, 1788 (1997).
- [5] S. Tarucha, D. G. Austing, T. Honda, R. J. van der Hage, and L. P. Kouwenhoven, "Shell filling and spin effects in a few electron quantum dot," *Phys. Rev. Lett.* 77, 3613 (1996).
- [6] C. W. J. Beenakker, "Theory of Coulomb-blockade oscillations in the conductance of a quantum dot," *Phys. Rev. B* 44, 1646 (1991).
- [7] J. Hubbard, "Electron correlations in narrow energy bands," *Proc. R. Soc. London A* 276, 238 (1963).
- [8] D. Loss and D. P. DiVincenzo, "Quantum computation with quantum dots," *Phys. Rev. A* 57, 120 (1998).
- [9] R. Hanson, L. P. Kouwenhoven, J. R. Petta, S. Tarucha, and L. M. K. Vandersypen, "Spins in few-electron quantum dots," *Rev. Mod. Phys.* 79, 1217 (2007).
- [10] J. R. Petta, A. C. Johnson, J. M. Taylor, E. A. Laird, A. Yacoby, M. D. Lukin, C. M. Marcus, M. P. Hanson, and A. C. Gossard, "Coherent manipulation of coupled electron spins in semiconductor quantum dots," *Science* 309, 2180 (2005).
- [11] J. M. Elzerman, R. Hanson, L. H. Willems van Beveren, B. Witkamp, L. M. K. Vandersypen, and L. P. Kouwenhoven, "Single-shot read-out of an individual electron spin in a quantum dot," *Nature* 430, 431 (2004).
- [12] F. H. L. Koppens, C. Buizert, K. J. Tielrooij, I. T. Vink, K. C. Nowack, T. Meunier, L. P. Kouwenhoven,

- and L. M. K. Vandersypen, "Driven coherent oscillations of a single electron spin in a quantum dot," *Nature* 442, 766 (2006).
- [13] W. G. van der Wiel, S. De Franceschi, J. M. Elzerman, T. Fujisawa, S. Tarucha, and L. P. Kouwenhoven, "Electron transport through double quantum dots," *Rev. Mod. Phys.* 75, 1 (2002).
- [14] T. Hayashi, T. Fujisawa, H. D. Cheong, Y. H. Jeong, and Y. Hirayama, "Coherent manipulation of electronic states in a double quantum dot," *Phys. Rev. Lett.* 91, 226804 (2003).
- [15] K. Ono, D. G. Austing, Y. Tokura, and S. Tarucha, "Current rectification by Pauli exclusion in a weakly coupled double quantum dot system," *Science* 297, 1313 (2002).
- [16] A. C. Johnson, J. R. Petta, J. M. Taylor, A. Yacoby, M. D. Lukin, C. M. Marcus, M. P. Hanson, and A. C. Gossard, "Triplet-singlet spin relaxation via nuclei in a double quantum dot," *Nature* 435, 925 (2005).
- [17] D. Goldhaber-Gordon, H. Shtrikman, D. Mahalu, D. Abusch-Magder, U. Meirav, and M. A. Kastner, "Kondo effect in a single-electron transistor," *Nature* 391, 156 (1998).
- [18] S. M. Cronenwett, T. H. Oosterkamp, and L. P. Kouwenhoven, "A tunable Kondo effect in quantum dots," *Science* 281, 540 (1998).
- [19] D. Schröer, A. D. Greentree, L. Gaudreau, K. Eberl, L. C. L. Hollenberg, J. P. Kotthaus, and S. Ludwig, "Electrostatically defined serial triple quantum dot charged with few electrons," *Phys. Rev. B* 76, 075306 (2007).
- [20] L. Gaudreau, A. Kam, G. Granger, S. A. Studenikin, P. Zawadzki, and A. S. Sachrajda, "A tunable few electron triple quantum dot," *Appl. Phys. Lett.* 95, 193101 (2009).
- [21] L. Gaudreau, S. A. Studenikin, A. S. Sachrajda, P. Zawadzki, A. Kam, J. Lapointe, M. Korkusinski, and P. Hawrylak, "Coherent coupling of two quantum dots embedded in an Aharonov-Bohm interferometer," *Phys. Rev. Lett.* 97, 036807 (2006).
- [22] M. C. Rogge and R. J. Haug, "Two-path transport measurements on a triple quantum dot," *Phys. Rev. B* 77, 193306 (2008).
- [23] M. C. Rogge and R. J. Haug, "Noninvasive detection of molecular bonds in quantum dots," *Phys. Rev. B* 78, 153310 (2008).
- [24] B. Michaelis, C. Emary, and C. W. J. Beenakker, "All-electronic coherent population trapping in quantum dots," *EPL (Europhysics Letters)* 73, 677 (2006).
- [25] M. Korkusinski, I. P. Gimenez, P. Hawrylak, L. Gaudreau, S. A. Studenikin, and A. S. Sachrajda, "Topological Hund's rules and the electronic properties of a triple lateral quantum dot molecule," *Phys. Rev. B* 75, 115301 (2007).
- [26] G. Granger, L. Gaudreau, A. Kam, M. Pioro-Ladrière, S. A. Studenikin, Z. R. Wasilewski, P. Zawadzki, and A. S. Sachrajda, "Three-dimensional transport diagram of a triple quantum dot," *Phys. Rev. B* 82, 075304 (2010).
- [27] M. Seo, H. K. Choi, S.-Y. Lee, N. Kim, Y. Chung, H.-S. Sim, V. Umansky, and D. Mahalu, "Charge frustration in a triangular triple quantum dot," *Phys. Rev. Lett.* 110, 046803 (2013).
- [28] R. Žitko, J. Bonča, and T. Pruschke, "Quantum phase transition in triple quantum dots," *Phys. Rev. B* 80, 245112 (2009).
- [29] W. G. van der Wiel, S. De Franceschi, J. M. Elzerman, T. Fujisawa, S. Tarucha, and L. P. Kouwenhoven, "Electron transport through double quantum dots," *Rev. Mod. Phys.* 75, 1 (2002).

- [30] R. Blankenbecler, D. J. Scalapino, and R. L. Sugar, "Monte Carlo calculations of coupled boson-fermion systems. I," *Phys. Rev. D* 24, 2278 (1981).
- [31] A.-P. Jauho, N. S. Wingreen, and Y. Meir, "Time-dependent transport in interacting and noninteracting resonant-tunneling systems," *Phys. Rev. B* 50, 5528 (1994).
- [32] C. W. J. Beenakker and A. A. M. Staring, *Phys. Rev. B* 46, 9667–9676 (1992).
- [33] Scarola V W and Das Sarma S 2005 *Phys. Rev. A* 71 032340
- [34] Z. H. Li, N. H. Tong, X. Zheng, D. Hou, J. H. Wei, J. Hu, and Y. J. Yan, *Phys. Rev. Lett.* 109, 266403 (2012).
- [35] R. P. Feynman and F. L. Vernon Jr., *Ann. Phys.* 281, 547 (2000).
- [36] J. Jin, X. Zheng, and Y. Yan, *J. Chem. Phys.* 128, 234703 (2008).
- [37] Y. Tanimura, *J. Chem. Phys.* 153, 020901 (2020).
- [38] Xu R X, Cui P, Li X Q, Mo Y and Yan Y J 2005 *J. Chem. Phys.* 122 041103
- [39] XuRX and YanYJ2007*Phys. Rev. E* 75 031107
- [40] Zheng X, Jin J S, Welack S, Luo M and Yan Y J 2009 *J. Chem. Phys.* 130 164708
- [41] Wen X G, Wilczek F and Zee A 1989 *Phys. Rev. B* 39 11413
- [42] Li Z H, Tong N H, Zheng X, Hou D, Wei J H, Hu J and Yan Y J 2012 *Phys. Rev. Lett.* 109 266403
- [43] Ye L Z, Wang X L, Hou D, Xu R X, Zheng X and Yan Y J 2016 *WIREs Comput. Mol. Sci.* 6 608